Comparison of Modelled and Measured Heat and Mass Transfer in a Liquid Desiccant Air-Conditioning System

Wael Mandow[1], Martin Mützel[1], Daniel Fleig[1], Andrew Lowenstein[2] and Ulrike Jordan[1]

[1] Institute of Thermal Engineering, Kassel University, Kurt-Wolters-Str.3, 34125-Kassel, Germany

[2] AIL Research Company, 57 Hamilton Ave, Hopewell, NJ 08525, USA

Abstract

In the presented research study, experimental and numerical investigations on the heat and mass transfer of the absorber and regenerator in a liquid desiccant air conditioning system (LDAC-system) were carried out. The absorber and regenerator are designed as a tube bundle heat and mass exchanger with corrugated media as wicking fins. An aqueous solution of lithium chloride ($LiCl-H_2O$) is used as desiccant. In the experiments all relevant in and outlet parameters of the air, desiccant solution, as well as cooling and heating water are measured for different inlet air humidity ratios in the absorber and for different heating water temperatures in the regenerator. Moreover, three different numerical models are applied to predict the heat and mass transfer in the absorber and regenerator, i.e. a physical model, a simplified single-node effectiveness model, and a multi-node effectiveness model. The impact of the inlet humidity ratio of the process air and the regeneration temperature on the moisture removal rate and the change of fluid temperatures were evaluated. In general, the results showed good agreements between measurements and numerical values.

Keywords: Liquid desiccant, Absorber, Dehumidifier, Air conditioning

1. Introduction

Desiccant dehumidification is used for air conditioning applications as well as product drying as an alternative to dehumidification with a vapor compression refrigeration cycle. It is possible to improve the performance of the process for a low set humidity and low set temperatures and to replace electrical by thermal energy demand (Yamaguchi et al. 2011; Qi et al. 2014; Mucke et al. 2016). An additional advantage of a desiccant air conditioning system compared to conventional systems are the pollution and bacterial control in the indoor air (Chung et al. 1995; Liu et al. 2015; Park et al.2017). Liquid desiccant air conditioning (LDAC) systems can be driven by lower regeneration temperatures compared to desiccant wheels, i.e. by temperatures lower than 80°C, to utilize solar energy or waste heat. Originally, liquid-desiccant absorbers and regenerators are designed as adiabatic packed beds with high flow rates of the liquid desiccant with an air to liquid mass flow ratio of about 1. The main disadvantage of packed-bed configurations are the risk of carryover of liquid droplets into the process air and a high pressure drop of the air Lowenstein et al. (2006).

As an alternative, the absorber and regenerator can be constructed as plate and tube-bundle heat and mass exchangers with a much higher air to liquid mass flow ratio in the range of MR ≈ 10 to 50. The absorption and regeneration process can be internally cooled and heated, respectively. These low flow systems can reach a higher dehumidification performance of the air and a larger spread of the LiCl mass fraction in the liquid compared to high flow and solid desiccant systems Lowenstein et al. (2006). Experimental investigations of the absorption process were carried out, for example by (Kessling et al. 1998; Lowenstein et al. 2006; Röben 1997; Jaradat, 2016). LDAC systems were used also for humidity control in post harvests, tea, hay drying and low-temperature crop drying in short time with less cost and without heat damage to seeds comparing with hot-air-drying (Sulardjaka et al. 2018; Addy et al. 2014; Khouzam, 2009). Furthermore, using liquid desiccant to dry gelcast parts reduced the drying time significantly without defects that occurred during conventional drying Barati et al. (2003).

In the following section the investigated liquid desiccant air conditioning system is described, followed by a brief description of three numerical models in section 3. In section 4, the evaluated variables are defined. Finally, in section 5, a series of experiments with a focus on the absorption and on the regeneration process are presented. Experimental results of the water vapor mass flow rate and the temperature rise and drop during the processes are presented and compared with results from the three numerical models.

© 2018. The Authors. Published by International Solar Energy Society
Selection and/or peer review under responsibility of Scientific Committee
doi:10.18086/eurosun2018.04.10 Available at http://proceedings.ises.org

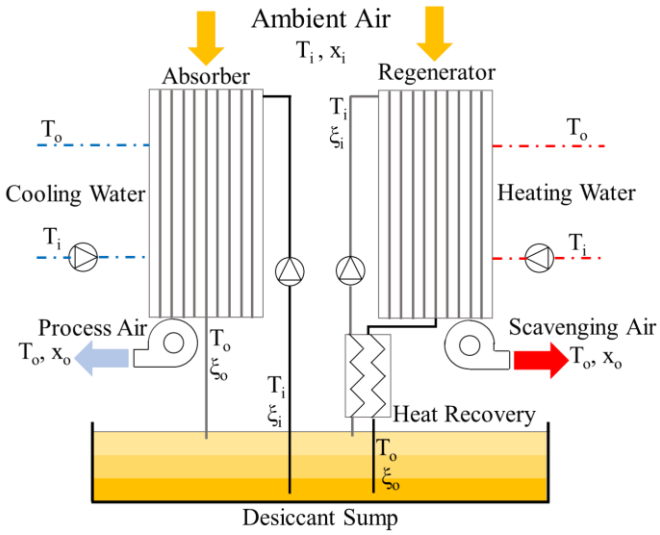

Fig. 1:Liquid desiccant air conditioning system (according to Andrusiak and Harrison, 2009), own drawing)

2. Investigated Liquid Desiccant System

A general scheme of a LDAC system is shown in Fig. 1. In the internally cooled absorber, air passes along a liquid desiccant film in cross-flow configuration. Water vapor is absorbed by the concentrated aqueous LiCl-solution due to its lower water vapor pressure above the solution compared to that in the air. Enthalpy of sorption (evaporation and dilution) is released during the process and transferred to the air and liquid desiccant as well as to the cooling water inside the absorber. The diluted desiccant is regenerated afterwards in an internally heated heat and mass exchanger, the regenerator. The absorber and regenerator are made of corrugated fiber glass sheets as wicking fins attached to cupronickel tube bundles, Fig. 3.

The LDAC system developed by AIL Research is shown in Fig. 2. It consists of an absorber with a volume of 105 litres and set-flow rates of 2000 m³/h (air) and 320 l/h (liquid desiccant). The volume of the regenerator is about 40 litres, the flow rates of the air and the desiccant are about 600 m³/h and 230 l/h, respectively. The system consists of a 50 litres desiccant sump, a heat recovery unit for the liquid desiccant, as well as pumps and fans with 1.27 kW_{el} nominal electrical power.

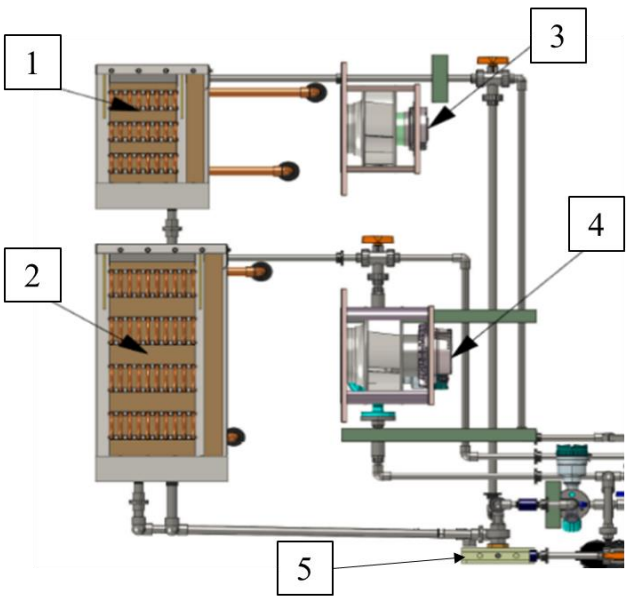

Fig. 2: LDAC-System, schematic diagram

1	Regenerator
2	Absorber
3	Outlet air ventilator
4	Inlet air ventilator
5	Heat recovery

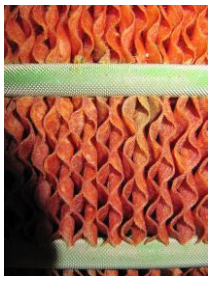

Fig. 3: Heat and mass exchanger design with corrugated wicking material

All relevant in- and outlet parameters of the air, desiccant solution, and cooling or heating water are measured. Tab. 1 shows measured parameters with uncertainties based on the manufacture's data.

Tab. 1: Estimated measurement uncertainty (based on instrument manufacture's data)

Instruments	Accuracy
Process-air	
Inlet and outlet temperature	±0.3 K
Inlet and outlet relative humidity	±1 % RH
Volume flow meter	±1.5 % of reading
Liquid desiccant	
Inlet and outlet temperature	±0.5 K
Inlet and outlet density	0.005 g/cm³
Mass flow meter	±0.15 % of reading
Cooling/ heating water	
Inlet and outlet temperature	±0.5 K
Mass flow rate	±0.5 % of reading

3. Numerical Models

Three numerical models are used to describe the heat and mass transfer and to compare the experimental with numerical results. All models assume steady-state operation, laminar-flow of all fluids, a uniform distribution of the air and of the desiccant solution on the plate surface and they assume that heat transfer to the surroundings is negligible.

a) Physical Model (FDM)

A three-dimensional physical model was developed to describe the heat and mass transfer of internally heated and cooled absorbers and regenerators. The model is based on the work by Mesquita et al. (2006).

The air and liquid desiccant are assumed to flow in cross-flow configuration. The algorithms are solved with a finite-difference method (FDM). In comparison to semi-empirical approaches (ε-NTU- model), the model applies solely physical fluid properties. In the presented study, 200 nodes in the two directions of the fluid flow and 50 nodes perpendicular to the flow directions were applied. Moreover, the film thickness of liquid desiccant is considered as constant, heat and mass transfer through convection perpendicular to flow-direction is neglected, and heat and mass transfer through conduction in flow-direction is neglected. The vapor pressure of the desiccant in dependency of fluid temperature and concentration is described by correlation from literature Conde, (2004).

The wicking fins are considered as flat plates with a distance of about 3 mm between the plates. The heat and mass transfer areas between air and desiccant as well as between liquid desiccant and cooling/heating water is assumed to be equal to the entire plate area.

Solely the heat transfer from the plate to the heating and cooling water is described with a semi-empirical parameter. A thermal conductivity of the plate of 0.21 W/mK and an equivalent plate thickness of 0.5 mm was assumed.

b) Single-node ε-NTU- model (EFFM)

A second model approach is simplified compared to the physical model. It is based on efficiency correlations with only one node for each fluid to describe the temperature and mass fraction at the phase boundary.

Stevens et al. (1989) already used an NTU-ε semi-empirical model derived from a model for a cooling tower. The model describes the heat and mass transfer within adiabatic packed bed absorber in a counterflow configuration. In the model the change of the liquid desiccant mass flow rate is assumed to be negligible, the variation of the saturation enthalpy is linear with the temperature, the Lewis number is assumed to be unity, and an ideal surface wetting is assumed.

In the presented study the model was further developed. Other than in the model by Stevens et al. (1989), the temperature and mass fraction is calculated at the phase boundary. The change of mass fraction of the liquid

desiccant is taken into account and the heat of dilution and vapor pressure are implemented as nonlinear correlations of temperature and mass fraction according to Conde, (2004). The Lewis number is defined from air properties (eq. 1), the mass transfer coefficient is calculated from the Lewis-number and the heat transfer coefficient according to (eq. 2), and NTU_β is given by (eq. 3). If the c_i is less or equal to unity in (eq. 7) then the LiCl-flow rate is used to calculate NTU_β., and if it is larger than unity, the air flow rate is applied.

$$Le = \frac{a_a}{D_a} \qquad \text{eq. 1}$$

$$\beta = \frac{\alpha \cdot D_a . Le^{\frac{1}{3}}}{\lambda_a} \qquad \text{eq. 2}$$

$$NTU_\beta = \frac{\beta \cdot A}{\dot{m}_{da}} \qquad \text{eq. 3}$$

Different areas can be considered in the model for the heat and mass transfer. Furthermore, the effect of non-uniform wetting can be considered by a wetting-factor. Different wetting factors can be applied for the heat and mass transfer area. Further, the temperature at the phase boundary is assumed to be equal to the liquid desiccant outlet temperature, and as characteristic length of the film, the inlet film thickness is considered.

As for the physical model, the wicking fins are considered as flat plates with a distance of about 3 mm between the plates. The heat and mass transfer area between air and desiccant is equal to the plate area. However, the heat transfer area between desiccant and cooling/heating water is assumed to be equal to the tube bundle area.

The effectiveness of heat transfer between interface and air as cooling or heating water depends on the dimensionless heat transfer coefficients NTU_a and NTU_w as given in eq. 4 and eq. 5:

$$\epsilon_{\alpha,a-sol} = 1 - exp(-\mathrm{NTU}_a) = 1 - exp\left(-\frac{\alpha A}{c_{Pa}\dot{m}_a}\right) \qquad \text{eq. 4}$$

$$\epsilon_{UA,w-Sol} = 1 - exp(-\mathrm{NTU}_W) = 1 - exp\left(-\frac{UA}{c_w \dot{m}_w}\right) \qquad \text{eq. 5}$$

The effectiveness of the mass transfer process for cross-flow configuration is calculated with eq. 6 and eq. 7:

$$\epsilon_{\beta,a-sol} = \frac{1}{c_i . NTU_{\beta i}} . \sum_{m=0}^{\infty} \left\{ \left[1 - \exp\left(-NTU_{\beta i}\right) . \sum_{j=0}^{m} \frac{1}{j!} NTU_{\beta i}^{j} \right] . \left[1 - \exp\left(-c_i NTU_{\beta i}\right) . \sum_{j=0}^{m} \frac{1}{j!} (c_i . NTU_{\beta i})^j \right] \right\} \qquad \text{eq. 6}$$

$$c_i = \frac{\dot{m}_{salt} . (X_{eq} - X_i)}{\dot{m}_{da} . (x_{a,i} - x_{a,eq})} \qquad \text{eq. 7}$$

c) Multi-Node ε-NTU- model (AILM)

The multi-node ε-NTU- model is a physical model based on the work by Kozubal et al. (2014). The plate is divided into eight elements in each direction and the mass and energy conservation equations are solved in each element. A Newton solver is used.

The model assumes negligible heat transfer resistance in the desiccant, and conduction and diffusion perpendicular to the plates only. It contains laminar developing flow transfer coefficients for both, heat and mass transfer from the bulk air to the air-liquid desiccant interface. The model is only applied for the absorber. It is described in Kozubal et al. (2014).

4. Evaluated Variables

The moisture removal rate $\dot{m}_v$ calculated from both, air and liquid desiccant, are calculated with eq. 8 and eq. 9:

$$\dot{m}_{v,air\ side} = \dot{m}_{da} \cdot (x_i - x_o) \qquad \text{eq. 8}$$

$$\dot{m}_{v,sol.side} = \dot{m}_{salt} \cdot (X_o - X_i) \text{ whereas } \quad X = \frac{1-\xi}{\xi} \qquad \text{eq. 9}$$

To evaluate the quality of the measurements, the mass balance and energy balance factors κ_m and. κ_e are defined according to eq. 10 and eq. 11, respectively. The deviation of the evaluated values from 1 is a quality measure of the experiments. $\dot{H}_{sorp.}$ is the sum of evaporation and dilution enthalpy flow.

$$\kappa_m = \frac{\dot{m}_{v,air\ side}}{\dot{m}_{v,sol.side}} \qquad \text{eq. 10}$$

$$\kappa_e = \frac{\dot{H}_{sorp.}}{\dot{Q}_{a,sen.} + \dot{Q}_{sol} + \dot{Q}_w} \qquad \text{eq. 11}$$

The regeneration specific heat input, RSHI, is defined as the heat demand for the liquid desiccant regeneration to remove one kg of moisture from the air, eq. 12

$$RSHI = \frac{\dot{Q}_{heat}}{\dot{m}_{v,sol.side}} \qquad \text{eq. 12}$$

5. Results and Discussion

Two test sequences were carried out to study the influence of the inlet air humidity ratio on the absorption process and the influence of the heating temperature on the regeneration process. The duration of each experiment was several hours however the presented time-averaged measurement date refers to sampling times of about 40 minutes, after the inlet desiccant density at the absorber and regenerator reached a constant value.

a) Absorption Process

Five experiments were performed to study the internally cooled absorption process with inlet air humidity ratios between 9.5 g_w/kg_{da} and 18.6 g_w/kg_{da}. The following inlet parameters were maintained constant for the five experiments: The air mass flow rate at about 2270 kg/h, the cooling water mass flow rate at about 1200 kg/h and the cooling water temperature at about 25.3 °C. The inlet temperature of the heating water into the regenerator was about 75°C and the hot water mass flow rate was about 1171 kg/h. Additional values are given in Tab. 2.

Tab. 2: Inlet conditions for different inlet humidity ratios, with a constant inlet air mass flow rate of (2270 ± 15) kg/h

$\dot{m}_{sol}$ in kg/h	351	337	320	308	307
ξ in kg_{salt}/kg_{sol}	0.30	0.30	0.32	0.36	0.39
T_{sol} in °C	32.8	32.3	32.4	31.7	31.7
T_a in °C	26.3	24.9	25.8	24.7	25.3
x_a in kg_w/kg_{da}	0.0186	0.0173	0.0153	0.0119	0.0095
$\dot{m}_w$ in kg/h	1201	1201	1201	1200	1200
T_w °C	25.2	25.3	25.3	25.3	25.3
κ_m	0.95	0.91	0.89	0.84	0.85
κ_e	0.97	0.97	0.98	0.96	0.93
RSHI in kJ/kg	3698	3884	3999	4327	4818

The moisture removal rate increases with increasing inlet air humidity ratio nearly linear, as shown in Fig. 4, due

to the increasing water vapor pressure difference between the air and the liquid desiccant. The dehumidification of the air rises from Δx_a= 3.6 g_w/kg_{da} to 6.1 g_w/kg_{da}. The maximal moisture removal rate measured on sorption side is above 14 kg/h for an inlet air humidity ratio of 18.6 g_w/kg_{da}.

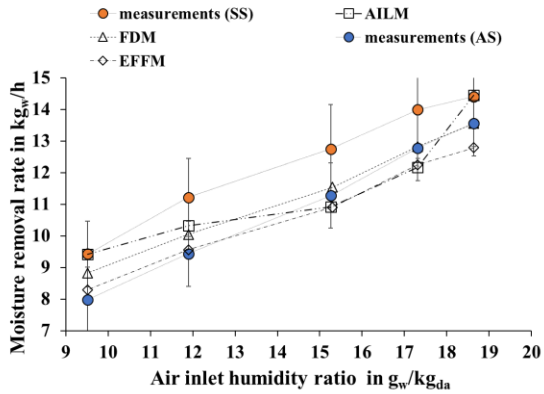

Fig. 4: Absorption process: Experimental and simulation results of the moisture removal rate over the inlet air humidity ratio.

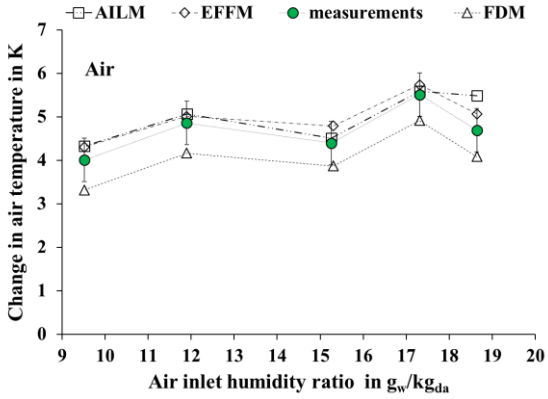

Fig. 5: Experimental and simulation results of the air temperature rise during the absorption process over the inlet air humidity ratio.

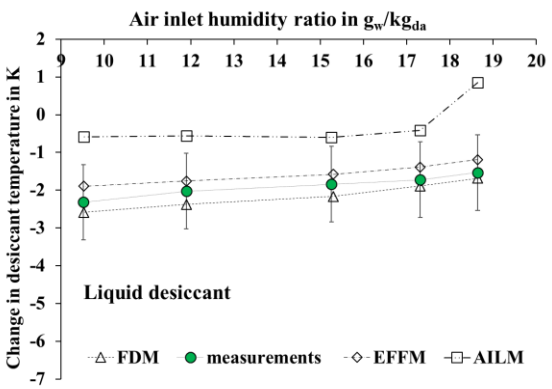

Fig. 6: Experimental and simulation results of the liquid desiccant temperature drop during the absorption process over the inlet air humidity ratio.

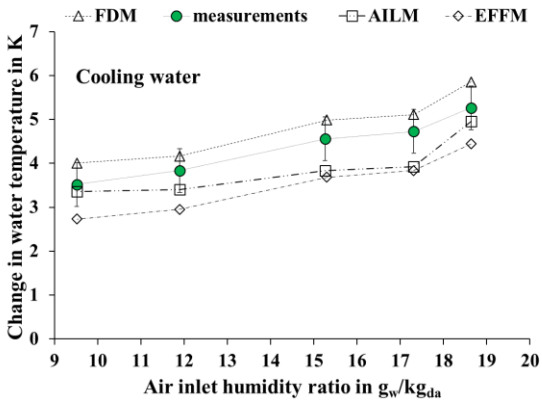

Fig. 7: Experimental and simulation results of the cooling water temperature rise during the absorption process over the inlet air humidity ratio.

The moisture removal rate $\dot{m}_v$ was calculated from measured data for both, air and liquid desiccant, with eq. 8 and eq. 9, respectively. The maximal deviation between the values is about 16%. This is mainly due to the uncertainty of the density and of the liquid desiccant outlet temperature. The change of the liquid desiccant mass fraction during the absorption process is relatively small, with a value of about 0.012 kg_{salt}/kg_{sol}.

If the calculated moisture removal rate is too high due to the density uncertainty, the simulated absorption enthalpy flow is too high, as well. This causes deviations between measured and simulated values not only of the moisture removal rate, but also of the change of the fluid temperatures.

The high uncertainty of the liquid desiccant outlet temperature is probably caused by the sensor position in the collecting pipe. The velocity of the liquid desiccant is very slow, the liquid accumulates at the lowest point, and cools down before it enters the collecting pipe.

A comparison between the measured values and the results of the three different numerical models described above, is shown in Fig. 4 to Fig. 7. In general, the experimental and numerical values of the moisture removal rate $\dot{m}_v$ show a good agreement. The numerical values are within the experimental uncertainty range. The trend of the FDM and EFFM results agrees very well with the trend of the measured data. The maximal deviation between numerical and measured values of the air side moisture removal rate $\dot{m}_{v,AS}$, are 11%, 6% and 18%, for the FDM, EFFM, and AILM, respectively.

The air and the cooling water are heated during the absorption process due to the absorption heat released, whereas the liquid desiccant is cooled due to its high inlet temperature compared to the air and cooling water inlet temperatures. The measured and simulated change in the air temperature is shown in Fig. 5. The FDM underestimates the measured increase of the air temperature, ΔT_a, with a maximal deviation of $\Delta T_a = \frac{\Delta T_{a,sim} - \Delta T_{a,meas}}{\Delta T_{a,meas}} = 17\%$, whereas the EFFM and AILM agree very well with experiments. The decrease of the liquid desiccant temperature for both, the FDM and EFFM, agrees well with experiments, with a maximal deviation of 17% and 22%, respectively, as shown in Fig. 6. The measured and simulated temperature rise of the cooling water, ΔT_w, agrees with the measured values for all models with a maximal deviation of 23%, as shown in Fig. 7.

The EFFM considered an overall heat transfer coefficient between the liquid desiccant and the cooling water in the range of 1152 W/K to 1462 W/K. The heat transfer coefficient between liquid desiccant and tube bundles is in the range of 825 W/m²K to 1160 W/m²K. With these values, the change of water temperature is calculated too low.

The FDM considered a higher overall heat transfer between liquid desiccant and water, with an equivalent heat transfer coefficient of about 2520 W/K. This causes an overestimation of the cooling water temperature rise and an underestimation of liquid desiccant as well as air temperature change. The regeneration specific heat input, defined as the regeneration heat to dehumidify the process air by 1 kg of water vapor, is in the range between about 3700 and 4800 kJ/kg for the experiments, with a heating water inlet temperature of about 75 °C and a hot water mass flow rate of about 1171 kg/h.

According to the measured values, about 70% of the heat flow (enthalpy of absorption and heat flow of desiccant) is transferred to the cooling water and about 30% to the air.

b) Regeneration Process

Four additional experiments were performed to study the internally heated regenerator process with inlet heating water temperatures between 50°C and 80°C, as shown in Tab. 3. The following inlet parameters were maintained constant for the experiments: The air mass flow rate at about 353 kg/h, the inlet air humidity ratio at about 12 g_w/kg_{da} and the heating water mass flow rate at about 980 kg/h. The moisture removal rate from the desiccant to the air and the change in fluids temperature as well as in liquid desiccant mass fraction were studied as a function of the heating water inlet temperature.

Tab. 3: Inlet conditions for different heating water temperatures, with a constant inlet air mass flow rate of (353 ± 2.8) kg/h

$\dot{m}_{sol}$ in kg/h	228	228.3	232	234
ξ_{sol} in kg_{salt}/kg_{sol}	0.28	0.30	0.33	0.37
T_{sol} in °C	27.1	27.9	29.8	31.0
T_a in °C	24.5	24.5	24.9	24.8
x_a in kg_w/kg_{da}	0.0124	0.012	0.0128	0.0123
$\dot{m}_w$ in kg/h	985	985	976	970
T_w in °C	50.1	60	70.2	80
κ_m	1.06	1.11	1.06	1.06
κ_e	1.14	1.01	1.01	1.05
$\dot{m}_{v,sol,side,\,abs}$ in kg/h	5.4	7.2	8.4	10
RSHI in kJ/kg	3583	3862	4074	4160

The moisture removal rate increases with increasing inlet heating water temperature, as shown in Fig. 8, due to the increasing water vapor pressure difference between the air and the liquid desiccant. The change in the liquid desiccant mass fraction increases from $\Delta\xi$= 0.004 kg_{salt}/kg_{sol} to 0.012 kg_{salt}/kg_{sol}. The maximal moisture removal rate is 7.3 kg/h (solution side) combined with a 3.3% point increase of the LiCl inlet mass fraction for an inlet heating water temperature of 80°C.

The maximal deviation of the moisture removal rate calculated from air side and the one calculated from the liquid desiccant is 11%. The main reason for the high deviations is the high uncertainty of the relative humidity measurements at high temperatures. Another reason for the uncertainties in the regeneration process are the high outlet temperatures of the liquid desiccant which cause higher heat losses to the surroundings compared to the values during the absorption process.

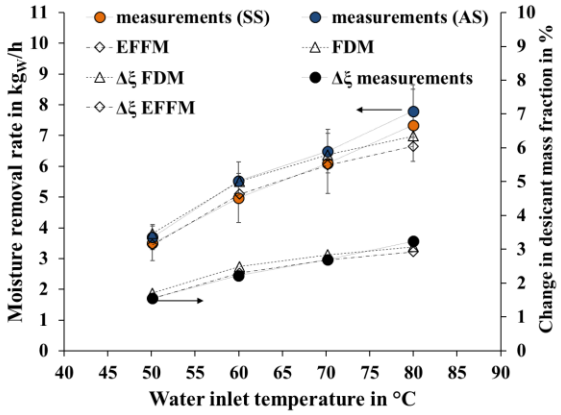

Fig. 8: Regeneration process: Moisture removal rate and increase of the LiCl mass fraction over the inlet heating water temperature

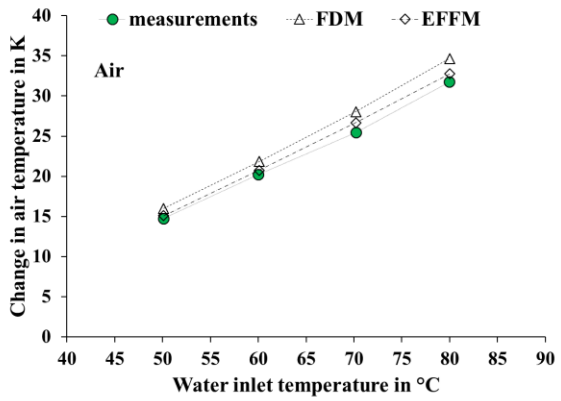

Fig. 9: Experimental and simulation results of the temperature increase of the air during regeneration over the inlet heating water temperature

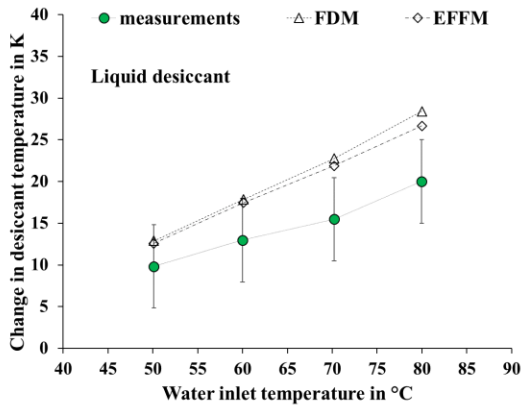

Fig. 10: Experimental and simulation results of the temperature increase of the desiccant during regeneration over the inlet heating water temperature

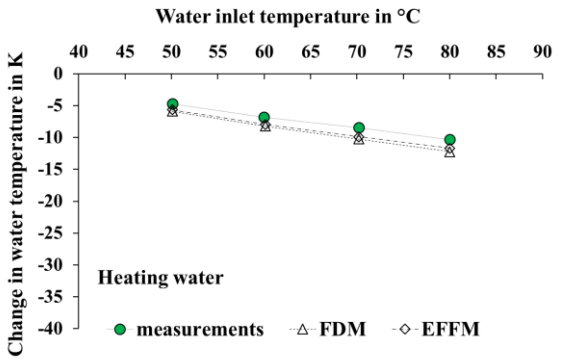

Fig. 11: Experimental and simulation results of the temperature decrease of the heating water during regeneration over the inlet heating water temperature

Fig. 8 shows in addition the comparison between the measured values with the results of the FDM and EFFM. As for the absorption process, the experimental and numerical values for the moisture removal rate show a good agreement and the simulated values are within the experimental uncertainty range. Also, the trend of the FDM and EFFM results agree well with the trend of the measured data. The maximal deviation between numerical and measured values of the air side moisture removal rate $\dot{m}_{v,AS}$, are 10% and 15% for the FDM and EFFM, respectively.

The air and liquid desiccant are heated during the regeneration process, whereas the heating water is cooled. The measured and simulated temperature increase of the air during regeneration is shown in Fig. 9. The models overestimate the measured increase of the air temperature, ΔT_a, with a maximal deviation of $\Delta T_a = \frac{\Delta T_{a,sim} - \Delta T_{a,meas}}{\Delta T_{a,meas}}$ by 5% (EFFM) and 10% (FDM). The models overestimate the liquid desiccant temperature rise with a maximal deviation of more than 40% compared to the measured results, Fig. 10. The latter can be partly explained by the unfavorable temperature sensor position, as described above. The measured temperature drop of the heating water, ΔT_w, agrees with the measured values for two models with a maximal deviation of 20% and 24%, respectively, Fig. 11.

According to the measured values, about 47% of the energy supplied by the heating water is used for the regeneration of the liquid desiccant, whereas 26% of the energy heats the liquid desiccant and about 27% heats the air.

6. Conclusions and Outlook

A liquid desiccant air conditioning system was investigated. The absorber and regenerator are constructed as tube bundle heat and mass exchangers with corrugated media as wicking fins. The mass transfer performance of the absorber and regenerator is evaluated in terms of the moisture removal rate $\dot{m}_v$ calculated from both, the air and the liquid desiccant side.

During the absorption process the moisture removal rate rises nearly linear with the air inlet humidity ratio, as expected for the investigated operating conditions. The maximum value reached is $\dot{m}_v$=14.4 kg/h with a change of the air humidity ratio of Δx = 6.1 g_w/kg_{da} for an inlet humidity ratio of 18.6 g_w/kg_{da} and the given reference conditions. About 70% of the released energy is transferred to the cooling water.

In a second step, the influence of the heating water temperature on the regeneration process was investigated. For a temperature of 80°C, the moisture removal rate evaluated from measurements is $\dot{m}_v$=7.3 kg/h with a change in the liquid desiccant mass fraction of $\Delta\xi$=0.012 kg_{salt}/kg_{sol} for the given reference conditions. Nearly half of the heat is used for the regeneration of the liquid desiccant, the remaining energy heats up the liquid desiccant and the air with nearly the same heat flow.

High deviations between the moisture removal rates calculated from the air side and from the solution side of up to 16% arise supposedly mainly from measurement uncertainties of the humidity ratio and liquid desiccant density.

The moisture removal rate and the change in the fluids temperature evaluated from measured data were compared with the results from three different numerical models. The results show good agreement for absorption as well as regeneration. The maximal deviation of the moisture removal rate between the models is 12% for the absorption process.

It was found that the effective areas for the heat and mass transfer play a significant role for a precise prediction of the three outlet temperatures. Whereas in a physical model both, the heat and mass transfer area are set equal to the plate area, in the single-node effectiveness model only the tube-bundle area was applied as heat transfer area. This leads to a higher heat transfer to the cooling water during the absorption process and a more effective heat transfer in the regeneration process for the physical model compared to the efficiency model.

Further investigations on the uncertainty of the measurements are required.

The single-node effectiveness model to describe the absorption and regeneration process will be used for a system model of the tested liquid desiccant air conditioning system.

Acknowledgements

The research project was financed by the German Federal Environmental Foundation (DBU) with a PhD scholarship and by the German Federal Ministry of Education and Research (BMBF) in the framework of the research project (OpenSorp, subsidy initiative storage research, code 03SF 0444). The authors would like to express their sincere thanks for the support. We express our gratitude to Mr. Janis Matthes and Mr. Simon Rabener for the operation of the liquid desiccant test unit and the recording of the measurement data

7. References

Addy, J.,Jaradat, M., Fleig, D., Vajen, V., Jordan, U., 2014. Experimentelle Untersuchung an einer offenen Absorptionsanlage zur Heutrocknung. DKV-Tagung 2014.

Andrusiak, M., Harrison, S., 2009. The modeling of a solar thermally-driven liquid-desiccant air conditioning system.

Barati, A., Kokabi, M., Famili, M. H.N., 2003. Drying of gelcast ceramic parts via the liquid desiccant method. Journal of the European Ceramic Society 23 (13), 2265–2272.

Chung, T.-W., Ghosh, T. K., Hines, A. L., Novosel, D., 1995. Dehumidification of Moist Air with Simultaneous Removal of Selected Indoor Pollutants by Triethylene Glycol Solutions in a Packed-Bed Absorber. Separation Science and Technology 30 (7-9), 1807–1832.

Conde, M., 2004. Properties of aqueous solutions of lithium and calcium chlorides: formulations for use in air conditioning equipment design. International Journal of Thermal Sciences 43 (4), 367–382.

Jaradat, M., 2016. Construction and Analysis of Heat-and Mass Exchangers for Liquid Desiccant Systems. Dissertation, Kassel university.

Kessling, W., Laevemann, E., Peltzer, M., 1998. Energy storage in open cycle liquid desiccant cooling systems. International Journal of Refrigeration 21 (2), 150–156.

Khouzam, K., 2009. Developing a Solar Drying Machine for Agricultural Products 2009. RIRDC Publication No 09/026.

Kozubal, E., Herrmann, L., Deru, M., Clark, J., Lowenstein, A., 2014. Low-Flow Liquid Desiccant Air-Conditioning: Demonstrated Performance and Cost Implications. Technical Report. 104 pp.

Liu, X., Guan, B., 2015. Experimental Study on the Filtration Efficiency of Structured Packing Air Handling Processors. Procedia Engineering 121, 2037–2043.

Lowenstein, A., Slayzak, S., Kozubal, E., 2006. A Zero Carryover Liquid-Desiccant Air Conditioner for Solar Applications, in: Solar Energy. ASME, pp. 397–407.

Mesquita, L.C.S., Harrison, S. J., Thomey, D., 2006. Modeling of heat and mass transfer in parallel plate liquid-desiccant dehumidifiers. Solar Energy 80 (11), 1475–1482.

Mucke, L., Fleig, D., Vajen, K., Jordan, U., 2016. Hybrid liquid desiccant air-conditioning systems: A conceptual study with respect to energy saving potentials. International Journal of Refrigeration 69, 64–73.

Park, J.-Y., Yoon, D.-S., Li, S., Park, J., Bang, J.-I., Sung, M., Jeong, J.-W., 2017. Empirical analysis of indoor air quality enhancement potential in a liquid-desiccant assisted air conditioning system. Building and Environment 121, 11–25.

Qi, R., Lu, L., Huang, Y., 2014. Energy performance of solar-assisted liquid desiccant air-conditioning system for commercial building in main climate zones. Energy Conversion and Management 88, 749–757.

Röben, J., 1997. Sorptionsgestützte Entfeuchtung mit verschiedenen wäßrigen Salzlösungen.

Stevens, D. I., Braun, J. E., Klein, S. A., 1989. An effectiveness model of liquid-desiccant system heat/mass exchangers. Solar Energy 42 (6), 449–455.

Sulardjaka, Nugroho, S., Suyanto, Fitriana, D. F., 2018. Investigation of Mechanical Properties of Al7Si/ SiC and Al7SiMg/SiC Composites Produced by Semi Solid Stir Casting Technique. MATEC Web of Conferences 159, 2025.

Yamaguchi, S., Jeong, J., Saito, K., Miyauchi, H., Harada, M., 2011. Hybrid liquid desiccant air-conditioning system: Experiments and simulations. Applied Thermal Engineering 31 (17-18), 3741–3747.

Nomenclature and Symbols

Symbol	Quantity	Unit
NTU	Number of transfer unit	
x	Humidity ratio	kg_w/kg_{da}
X	water content in salt	kg_w/kg_{LiCl}
ξ	Mass fraction	
Le	Lewis number	
V	volume	m³
$\dot{m}$	Mass flow rate	kg/h
c_p	Specific heat capacity	kJ/kg.K
A	Transfer area	m²
D	Diffusion coefficient	m²/s
a	Thermal diffusivity	m²/s
U	Overall heat transfer coefficient	W/m²K

$\dot{H}_{sorp.}$	Sorption enthalpy flow	W
MR	Mass flow rate air/Mass flow rate solution	
RSHI	Regeneration specific heat input	kJ/kg_V

Greek symbols

ε	effectiveness	
β	Mass transfer coefficient	kg/m²s
α	Heat transfer coefficient	W/m²K
κ_e	Energy balance factor	
κ_m	Mass balance factor	

subscripts

a	Air
da	Dry air
sol	Liquid desiccant
w	Cooling or heating water
i	inlet
o	outlet
Eq.	equilibrium
v	Water vapour
sat	saturated
eff	effective
sen	sensible
abs	absorption